



# Use of ram extruder as a combined rheo-tribometer to study the behaviour of high yield stress fluids at low strain rate

Arnaud Perrot, Yannick Mélinge, Damien Rangeard, Francesca Micaelli,  
Patrice Estellé, Christophe Lanos

## ► To cite this version:

Arnaud Perrot, Yannick Mélinge, Damien Rangeard, Francesca Micaelli, Patrice Estellé, et al.. Use of ram extruder as a combined rheo-tribometer to study the behaviour of high yield stress fluids at low strain rate. *Rheologica Acta*, 2012, 51 (8), pp.743-754. 10.1007/s00397-012-0638-6 . hal-00716752

**HAL Id: hal-00716752**

**<https://hal.science/hal-00716752>**

Submitted on 17 Sep 2012

**HAL** is a multi-disciplinary open access archive for the deposit and dissemination of scientific research documents, whether they are published or not. The documents may come from teaching and research institutions in France or abroad, or from public or private research centers.

L'archive ouverte pluridisciplinaire **HAL**, est destinée au dépôt et à la diffusion de documents scientifiques de niveau recherche, publiés ou non, émanant des établissements d'enseignement et de recherche français ou étrangers, des laboratoires publics ou privés.

# USE OF RAM EXTRUDER AS A COMBINED RHEO-TRIBOMETER TO STUDY THE BEHAVIOUR OF HIGH YIELD STRESS FLUIDS AT LOW STRAIN RATE

A. Perrot<sup>1\*</sup>, Y. Mélinge<sup>2</sup>, D. Rangeard<sup>2</sup>, F. Micaelli<sup>3</sup>, P. Estellé<sup>3</sup>, C. Lanos<sup>3</sup>

(1) Laboratoire d'ingénierie des Matériaux de Bretagne, Université de Bretagne Sud, Université Européenne de Bretagne - Centre de Recherche Christiaan Huygens, BP 92116, 56321 LORIENT Cedex, France

(2) LGCGM, INSA Rennes, Université Européenne de Bretagne, 20 avenue des buttes de Coësmes, Rennes, France

(3) LGCGM, Université de Rennes 1, Université Européenne de Bretagne, 3 rue du clos courtel, Rennes, France

\*: Corresponding author

**Arnaud Perrot**

**Mail:** [arnaud.perrot@univ-ubs.fr](mailto:arnaud.perrot@univ-ubs.fr) ; **Tel:** +33 2 97874577; **Fax:**+33 2 97874576

## **Abstract:**

We propose in this work to provide an efficient and simple extruder device able to evaluate the rheological and tribological behaviour of high yield stress fluids, such as extrudible materials. An extruder able to measure simultaneously both the friction force acting on the extruder wall and the total extrusion force is developed. Based on previous studies, an efficient and accurate method of data analysis is then proposed and applied in order to obtain both a flow curve and a tribological law. Experimental tests are performed on soft modelling clay, kaolin paste and cement-based materials. Results are compared to conventional rheometry measurements. This comparison helps to evaluate the accuracy of the proposed experimental device and procedure.

**Keywords:** Extrusion, rheology, tribology, yield stress.

27 **Nomenclature**

- 28 d: Die orifice diameter (m)
- 29 D: Extruder barrel diameter (m)
- 30 F: Total extrusion force recorded at the ram (N)
- 31  $F_{fr}$ : Friction force on the extruder barrel (N)
- 32  $F_{pl}$ : Shaping force required to ensure the flow in the die land (N)
- 33  $F_{pl1}$ : Contribution of  $F_{pl}$  induced by the bulk deformation in the shaping zone (N)
- 34  $F_{pl2}$ : Contribution of  $F_{pl}$  induced by the friction acting along the dead zone surface (N)
- 35  $F_{pl3}$ : Contribution of  $F_{pl}$  induced by the friction along the exit orifice surface (N)
- 36  $h_c$ : Height of the cylinder tool (m)
- 37  $h_v$ : Height of the vane tool (m)
- 38  $k_{fr}$ : Apparent friction factor ( $\text{Pa} \cdot (\text{s} \cdot \text{m}^{-1})^{n_{fr}}$ )
- 39  $k_s$ : Shear consistency -Herschel-Bulkley behaviour ( $\text{Pa} \cdot \text{s}^n$ )
- 40  $K_w$ : Wall friction stress (Pa)
- 41  $K_{w0}$ : Wall friction yield stress (Pa)
- 42  $L_B$ : Length of remaining billet (m)
- 43  $L_{dz}$ : Static or dead zone length (m)
- 44  $L_O$ : Exit orifice length (m)
- 45 m: Ratio of the wall friction stress to the bulk shear stress
- 46 M: Maximum torque recorded during vane tests (N.m)
- 47  $n_{fr}$ : Friction index
- 48  $n_s$ : Shear flow index -Herschel-Bulkley behaviour
- 49  $R_c$ : Radius of the cylinder (m)
- 50  $R_t$ : Valley to peak value of the surface roughness profile (m)
- 51  $R_v$ : Radius of the vane tool (m)

52  $V$ : Ram velocity ( $\text{m.s}^{-1}$ )

53  $V_i$ : Velocity at the interface between extruder wall and material billet ( $\text{m.s}^{-1}$ )

54  $\dot{\gamma}$ : Shear rate ( $\text{s}^{-1}$ )

55  $\theta$ : Conical die entry defined as half the included angle of the dead zone

56  $\sigma_0$ : Bulk elongational yield stress (Pa)

57  $\tau$ : Bulk shear stress (Pa)

58  $\tau_0$ : Bulk shear yield stress (Pa)

59

## 60 **1. Introduction**

61

62 Extrusion is a highly efficient forming process used in a wide range of industries such as food  
 63 engineering, ceramics, pharmaceuticals, building materials, etc. The extrusion flow properties  
 64 are directly linked to the material rheology and tribology. An accurate evaluation of the  
 65 rheological and tribological behaviour of the extruded materials is crucial in order to optimize  
 66 the process.

67 In Händle's book on ceramics extrusion, ram extrusion is defined as a discontinuous shaping  
 68 process in which a plastic material is pushed through a die or matrix by a piston, whereby the  
 69 geometry of the die determines the extrudates profiles (Doll et al. 2007). The use of a ram  
 70 extruder as a rheometer has already been studied many times (Avitzur 1983; Basterfield et al.  
 71 2005; Benbow and Bridgwater 1993; Hill 1950; Horrobin 1999; Mimoune and Aouadja 2004;  
 72 Toplak et al. 2007; Li and Bridgwater 2000; Benbow et al. 1991).

73 In this study, we focus on the development and the use of a ram extruder device dedicated to  
 74 the study of the rheological and tribological behaviour of high yield stress fluids. The  
 75 developed apparatus is able to provide independently the wall shear stress at the  
 76 paste/extruder barrel interface and the pressure required in the die land while common

77 capillary rheometer only provides the total pressure drop required to ensure the flow in the die  
78 land. This is of great interest because data analysis of common capillary tests requires  
79 assumptions or tests performed with different die geometry in order to separate the pressure  
80 drop contribution due to the wall friction from the contribution due to plastic deformation in  
81 the shaping area.

82 In a first approach, Benbow and Bridgwater (Benbow and Bridgwater 1993) and Hill (Hill  
83 1950) have used the ram extrusion geometry as a tool providing a comparative parameter (for  
84 example “extrusion pressure” or “bulk yield stress”) which is directly linked to the die  
85 pressure drop. These studies have contributed to improve the ideal work equation used for  
86 plastic materials. The effect of ram velocity can also be studied with such data analysis  
87 methods (Benbow and Bridgwater 1993).

88 Those methods only provide comparative parameters which depend on the ram extruder  
89 geometry as shown by recent studies (Basterfield et al. 2005; Toplak et al. 2007). For  
90 example, the measured values of extensional yield stress can be far larger than the extensional  
91 yield stress of the material computed from rotational rheometry (Srinivasan et al. 1999; Zhou  
92 and Li 2005a). However, those methods are the most widely used with a ram extruder and  
93 have been used in several studies to analyse the extrudability of materials or to evaluate the  
94 material’s flow behaviour (Alfani and Guerrini 2005; Cheyne et al. 2005; Martin et al. 2006;  
95 Mascia et al. 2006; Rahman et al. 2002; Srinivasan et al. 1999; Zhou and Li 2005a; Zhou and  
96 Li 2005b).

97 For plastic material and using plastic theory and slip lines analysis, several studies provide  
98 more accurate modelling of the force required to overcome the diameter variation using the  
99 material elongational yield stress. Those methods require assumptions on the velocity field,  
100 slip line design and limit conditions. This was attempted by Horrobin (Horrobin 1999;

101 Horrobin and Nedderman 1998), Avitzur (Avitzur 1983) or Kobayashi and Thomsen  
102 (Kobayashi and Thomsen 1963).

103 In recent studies, theoretical frames have been developed to compute intrinsic rheological  
104 parameters such as yield stress, consistency or flow index from extrusion tests.

105 For example, Basterfield et al. (Basterfield et al. 2005) proposed an adaptation of the Gibson  
106 equations (Gibson 1988) which is used to compute the viscosity and flow index of a power  
107 law fluid from orifice extrusion force data. The authors assume a radially convergent flow  
108 from the extruder body to the exit die. The proposed model assumed the converging flow to  
109 be purely elongational.

110 Toplak et al. (Toplak et al. 2007) have recently developed a new method to compute the yield  
111 stress of a material from its gravity draining through an orifice. The authors assume the flow  
112 to be similar to the Poiseuille flow through a cylindrical barrel with a diameter equal to the  
113 exit die one. The proposed model assumes a shear flow and was successfully applied to wide  
114 bore capillary rheometer with small die cross sections.

115 Extrusion is also greatly influenced by the material tribology as shown in several studies  
116 (Estellé et al. 2006; Mankar et al. 2004; Perrot et al. 2006; Toutou et al. 2005). Friction may  
117 occur in the die land area (Benbow and Bridgwater 1993), but also between the extruder  
118 barrel and the material billet as shown in (Mankar et al. 2004; Perrot et al. 2006). Moreover,  
119 for high solid volume content materials such as cement-based material, friction forces are the  
120 the most important resistant force to overcome in order to ensure the extrusion flow. As a  
121 consequence, it is crucial to study what happened far from the die land. This means that the  
122 tribological behaviour of the material has to be determined.

123 This leads to the conclusion that the total extrusion force can be split into two contributions:  
124 the force required to overcome the diameter decrease and the force required to overcome the  
125 friction force acting on the extruder barrel.

In this study, we propose to design a novel ram extruder which makes it possible to study both rheological and tribological behaviour of high yield stress fluids (shear yield stress larger than 1 kPa). The developed apparatus is able to measure simultaneously the friction force between the extruder and the material billet and the total extrusion force. This extruder is then tested on three different materials: a cement-based material, a kaolin clay paste and commercial soft modelling clay. An adaptation of the model developed by Basterfield et al. is done (Basterfield et al. 2005) to obtain an accurate estimation of the rheological modelling parameters taking into account the friction acting along the dead zone (which acts as a tapered die).

## **2. Materials and protocols**

### **2.1. Tested materials**

Three pasty materials are tested. They exhibit a yield stress ranging from 15 to 50 kPa. The first one is a commercial soft modelling clay which is known to exhibit a viscoplastic behaviour with negligible elastic properties after short compression (Estellé et al. 2006). The second material is a mix of kaolin clay powder and water (water/kaolin mass ratio equal to 38%). The kaolin clay used is a Powdered Polwhite BB from Imerys (Kaolins de Bretagne, Ploemeur, France). The largest clay grain size is close to 40  $\mu\text{m}$ . The mass mean kaolin grain size is close to 9  $\mu\text{m}$ . The third material is a cement-based material containing a large amount of fly ash. The dry powder consists in a mix of 70% of fly ash and 30% of cement. The fly ash has an optimized grain size distribution (mix between micronised and natural) and the cement is an Italcementi type I 52.5 R. The liquid phase is composed by tape water (96 % in mass) and methylcellulose 4% in mass). Such admixture is a polymeric suspension acting as a viscosity enhancer agent in order to reduce drainage. Tests on cement-based paste are

performed without delay after mixing in order to avoid rheological changes due to chemical effects.

In the present study, the paste compressibility has been neglected. This assumption is supported by two main reasons. Firstly, the study does not concern highly viscous polymer melts which are very sensitive to pressure (Park et al. 2008; Dealy 1995). Secondly, the compressibility effects in the die land remain limited because the recorded pressures are relatively low (under 500 kPa). Such hypothesis seems to be relevant in the present study but it cannot be held in high pressure capillary flow of firm polymer pastes (Mitsoulis and Hatzikiriakos 2009; Mitsoulis et al. 2007).

The rheological behaviour of the three tested pastes is visco-plastic. It is important to note that the extruder is efficient only if the tested material remains homogeneous. Thus, it is crucial to check that no drainage occurs during the test. A possible drainage may prohibit the use of the tested device at low ram velocity (Martin et al. 2006; Mascia et al. 2006; Perrot et al. 2007; Perrot et al. 2009; Yu et al. 1999). This can be done by measuring the densities of both the extrudates and the remaining material in the extruder.

Reference shear flow measurements have been independently performed under isothermal conditions (20°C) using a Brookfield Soft/Solid tester equipped with a vane geometry in an infinite cup (200x200 mm<sup>2</sup>). This type of cup is used to circumvent the wall slip artefact. The radius of the four-bladed vane geometry is 4 mm and its height is 8 mm. The shear yield stress is estimated at low shear rate using the stress growth test (Liddell and Boger 1996). Tests are conducted under a rotation rate controlled mode. The tool rotation rate is set at 0.01 rad.s<sup>-1</sup>. This rotation rate is in agreement with the Liddell and Boger protocol and allows for an accurate determination of the yield stress (viscous effects neglected). As proposed by Estelle et al., the end effect is neglected (Estellé et al. 2008). The shear yield stress  $\tau_0$  is deduced using equation (1).



$$\tau_0 = \frac{M}{2\pi R_v^2 h_v} \quad (1)$$

where  $M$  is the maximum recorded torque and  $R_v$  and  $h_v$  the vane radius and height.

Vane measurements provide shear yield stress of  $15 \pm 1$  kPa,  $25 \pm 2$  kPa and  $50 \pm 4$  kPa for the cement based material, the kaolin paste and the soft modelling clay, respectively. Because such materials can exhibit viscous behaviour, a Herschel-Buckley model is used in the following, making it possible to describe possible shear-thinning or shear-thickening behaviour:

$$\tau = \tau_0 + k_s \dot{\gamma}^{n_s} \quad (2)$$

where  $\dot{\gamma}$ ,  $k_s$  and  $n_s$  are respectively the shear rate, the consistency and the flow index.

For the tribological behaviour, it has been shown that high yield stress fluids exhibit a friction yield stress value (Roussel and Lanos 2003). The main hypothesis is based on purely plastic flow theory where the friction stress against a steel smooth surface (roughness height,  $R_t$  up to  $3 \mu\text{m}$ ) is considered to be a fraction of the shear stress which strongly depends on the surface roughness (Avitzur 1983; Horrobin 1999). This assumption has been successfully applied to model the squeeze flow of viscoplastic materials (Sherwood and Durban 1996, 1998). The friction yield stress, denoted  $K_{w0}$ , is measured using the stress growth test procedure used for the shear yield stress measurement (low rotating velocity to avoid velocity influence) replacing the vane tool by a smooth steel cylinder ( $R_C = 4$  mm and  $h_C = 4$  mm). The friction yield stress is also determined by means of the back extrusion technique. The surface roughness of the back extrusion device and the extruder barrel are equivalent (Perrot et al. 2011). The soft modelling clay exhibits a friction yield stress value of  $30 \pm 2$  kPa with both techniques. For kaolin, the measured friction yield stress value is  $9.5 \pm 0.5$  kPa with the rotating smooth cylinder and  $9 \pm 1$  kPa with the back extrusion technique. This shows that

both techniques provide equivalent results. The friction yield stress has not been measured for the cement-based mix.

Then the velocity effect is highlighted using an analogy with the rheological behaviour. A Herschel-Buckley-like equation has already been used by Benbow and Bridgwater to analyse the friction stress inside a die capillary geometry (Benbow and Bridgwater 1993). The proposed equation can be written as follows:

$$K_w = K_{w0} + k_{fr} \cdot V_i^{n_{fr}} \quad (3)$$

Where  $V_i$  is the velocity at the interface,  $k_{fr}$  is the apparent friction factor and  $n_{fr}$  the friction index.

## **2.2. High yield stress materials flowing through ram extruder**

In order to develop an efficient extruder to study the material flow behaviour, it is crucial to understand the flow properties of a high yield stress fluids in an axisymetrical ram extruder. The properties of extrusion flow of high yield stress fluids have already been studied through various techniques: MRI (Götz et al. 2003; Rabideau et al. 2010; Barnes et al. 2006), positron emission particle tracking (Wildman et al. 1999), visual observations (Hill 1950; Perrot et al. 2007) or numerical simulations (Horrobin 1999; Horrobin and Nedderman 1998; Jay et al. 2002; Zienkiewicz et al. 1977). From those studies conducted at low shear rate, axisymetrical extrusion flow can be divided into three parts (Fig. 1):

- A plug flow located in the extruder barrel where the paste seems to slip along the wall. This slippage induces friction force that should be overcome to ensure the extrusion flow.
- A tapered static zone where the material remains blocked around the die entry. This area is called the “dead zone”. It is assumed that the dead zone acts as a conical or tapered entry die as proposed in previous studies (Basterfield et al. 2005; Horrobin 1999).

- A forming zone, located inside the conical dead zone, where the material billet diameter decreases. This zone is called the “shaping zone”.

Thus, it appears obvious to introduce representative force for each part of the flow where material advance and forming occurs (as shown in figure 1):

- The shaping force required to give its final shape to the material in the shaping zone, denoted  $F_{pl}$  has been the subject of numerous studies (Avitzur 1983; Basterfield et al. 2005; Benbow and Bridgwater 1993; Gibson 1988; Hill 1950; Horrobin 1999; Horrobin and Nedderman 1998; Kobayashi and Thomsen 1963; Benbow et al. 1991) .

- The wall friction force  $F_{fr}$ , developed along the extruder body  $F_{fr}$  is linked to the friction stress value  $K_w$ .

The reference pressure is the external pressure  $P_{atm}=0$ . As described in figure 1,  $L_{dz}$  denotes the dead zone length and  $L_B$  is the friction length. The length of the dead zone is known to depend on both die and extruder body diameters. It is commonly considered that the conical dead zone is characterised by a  $\pi/4$  angle. In his study, Basterfield et al. have showed that the variation of this angle between  $\pi/3$  and  $\pi/6$  has only little effect on the extrusion pressure. As a result, the dead zone length can be modelled as follows (Basterfield et al. 2005; Mascia et al. 2006):

$$L_{dz} = \frac{D-d}{2} \quad (4)$$

This assumption is in agreement with the modelling results reported in previous studies (Avitzur 1983; Basterfield et al. 2005; Benbow and Bridgwater 1993; Gibson 1988; Hill 1950; Horrobin 1999; Horrobin and Nedderman 1998; Kobayashi and Thomsen 1963). However,  $L_{dz}$  is also largely influenced by the roughness of the extruder barrel and die surface. As shown by Horrobin (Horrobin 1999), the roughness of the extruder walls largely influences the dead zone length and form. As a result, it is required to measure the dead zone length after extrusion to check if eq. (4) is valid for a given extruder/material couple.

As shown in figure 2, the dead zone length can also be measured from the visualisation of the soft modelling clay remaining in the extruder after extrusion. The dead zone presents little curvature however we assumed that both dead zone length and form are close to the modelled conical one.

### **2.3. Extrusion device and tests**

The developed ram extruder shown on figure 3 must be able to measure simultaneously both force contributions: the shaping force acting in the shaping zone and the friction forces acting on the extruder barrel.

The extruder barrel consists of a vertical steel barrel of 300 mm in length and 43.3 mm in diameter (denoted  $D$ ) placed under a controlled velocity load frame. The surface roughness of the barrel is  $R_t = 3 \mu\text{m}$  and represents the maximum peak to valley height of the roughness profile. A nylon ram is used to push the material inside the barrel, ensures a uniform pressure on the material and avoids liquid drainage upward the ram. This ram is equipped with a 20 kN load cell (with a 1 N accuracy) in order to measure the total extrusion force  $F$  required to overcome both frictions on the extruder barrel and shaping force in the die land.

The extruder barrel is placed on a novel die system which is fixed on the load frame. This system allows measuring the friction force acting along the barrel wall. The bottom of the extruder barrel and the top of the die system are both equipped with similar circular shoulders of diameter 100 mm. The shoulders are perforated by three holes (diameter 6 mm –  $120^\circ$  oriented) and connected using three small perforated cylindrical 2 kN load cells which are centred on the holes (diameter 20 mm, hole diameter 6 mm, thickness 3 mm, and 1 N accuracy). Those load cells are pre-stressed by a screw-bolt system.

During extrusion, the material billet induces a wall friction stress on the extruder barrel which tends to move the barrel downward toward the die and consequently squeezes the three load

cells. The sum of the three recorded forces is considered to be equal to the friction force  $F_{fr}$  acting on the extruder barrel surface.

Then, the shaping force can be deduced from the measured values of both the total extrusion force measured at the ram and the friction force measured by the load cells supporting the barrel.

The friction force measurement requires some geometrical adjustments:

- The length of the barrel should be greater than its diameter in order to give sufficient surface for the measurement of the friction acting on the barrel surface.
- The die diameter should be at least 10 times the maximum particle diameter in case of suspensions extrusion.
- According to eq. (4), low extrusion ratio  $d/D$  (less than 0.1) leads to high value of  $L_{dz}$ .

Then the dead zone may enter the friction measurement zone. In this case, use of wide bore capillary rheometer analysis should be preferred (Toplak et al. 2007).

This third geometrical limitation is crucial. If the dead zone is long enough to enter the barrel, the force measured by the three small load cells will not exactly correspond to the friction linked to the moving material and then will not provide an accurate value of the wall friction stress. In order to avoid this measurement artefact, a zone of 20 mm in length is placed between the exit orifice (square angle die) and the extruder barrel. With the used die diameters (denoted  $d$ ) of 8, 15 and 20 mm and using eq. (4) the computed dead zone length ranges from 11.5 to 17.65 mm (which is less than 20 mm). This ensures that the dead zone does not obstruct the movement due to the friction force at the flowing material/barrel interface.

The die land is 8 mm long. Wall Friction on the die land surface has to be subtracted from the measured shaping force in order to study the work done in the conical zone where the material diameter is shaped. The procedure will be presented in the shaping force analysis section.

A 55.3 mm diameter extrusion barrel with common square angle dies is also used in addition to the 43.3 mm diameter developed extruder. It is done to verify if the proposed data analysis depends on the extruder geometry.

Extrusion tests are carried out under a load frame ensuring a constant ram velocity ranging from  $0.1 \text{ mm.s}^{-1}$  to  $8.33 \text{ mm.s}^{-1}$ .

The material billet length is controlled and ranges from 120 to 200 mm depending on the test.

Both extruder barrels can be used with three different square angle exit dies that allow for performing tests at the same extrusion ratios (i.e.  $d/D$  equals to 0.18, 0.34 and 0.45). The final volume and mass are measured and the computed apparent density is compared to the theoretical density.

### **3. Experimental results analysis**

#### **3.1. Extruder device validation and force data analysis**

An illustration of the total extrusion force versus the remaining billet length is presented in figure 4. The curve can be split into three distinct parts. The first part consists in the flow initiation. At the beginning of extrusion, the billet length is at its maximum. When the ram starts to move, the billet is compacted. As a result, the recorded extrusion force dramatically increases. We consider that this step ends when the extrusion force reaches its maximal value. Then the second part begins. The extrusion force starts to linearly decrease as the ram advances (i.e. as the remaining billet length decreases). Such particular force versus billet length evolution can be observed because the fluid is mainly plastic and remains homogeneous during the extrusion time. In addition, this linear evolution is linked to the linear decrease of the billet length due to the constant ram velocity. As the billet length linearly reduces, the surface of friction between the extruder barrel wall and the material billet

linearly decreases. This allows us to write the following relationship which provides us the friction stress denoted  $K_w$  from a simple force balance equation:

$$K_w = \frac{1}{\pi \cdot D} \frac{dF}{dL_B} \quad (5)$$

Where  $F$  is the extrusion force and  $L_B$  is the remaining billet length as defined in figure 1.

The third part of the curve begins when the evolution of the force versus the billet length variation becomes non linear. This happens when the ram is near the die land area and squeezes the static zone. The recorded force can reach a constant value or can increase with the billet length decreasing. Then, the extrusion test is stopped when the billet length is equal to 5 mm.

The analysis of the extrusion force curve allows us to restrain the data analysis to the second part of the curve (linear decrease of the force) which provides us a friction stress value. The use of the developed extruder provides the evolution of both the friction force along the extruder barrel wall and the total extrusion force as shown in figure 5. The slopes of the friction force curve and total force curve are very close (deviation of 3%). This indicates that the two measurements provide the same information as both curves allow for the computation of the friction stress  $K_w$  using eq. (5). Testing visco-plastic non compressible material helps us to show the efficiency of the two data analysis procedures. The effects of both shaping and friction force along the extruder barrel on the total extrusion force is highlighted. Finally, with the illustration given in figure 5, the computation of the friction stress  $K_w$  with eq. 5 can be performed with the data obtained from both the total extrusion force and the measured friction force data.

The difference between the total extrusion force  $F$  and the friction stress  $F_{fr}$  provides a quasi-constant value which is not influenced by the ram advance as shown in figure 5. This force is considered to be equal to the shaping force  $F_{pl}$  required to reduce the billet diameter from  $D$  to  $d$ . The resulting force value, denoted  $F_{pl}$  can be used to compute an elongational or a shear

yield stress and a velocity factor which can be linked to the consistency and the flow index of the tested material (Avitzur 1983; Basterfield et al. 2005; Benbow and Bridgwater 1993; Horrobin 1999; Kobayashi and Thomsen 1963; Mimoune and Aouadja 2004; Toplak et al. 2007; Hill 1950). In addition,  $F_{pl}$  can be computed from the total extrusion force curve when the remaining billet length is equal to the dead zone length  $L_{dz}$  estimated with eq. (4). Eq. (4) provides  $L_{dz}$  value equal to 13.65 mm. At this value of billet length, the total extrusion force is equal to 716 N. This force is close to the difference between the measured total extrusion force and the measured friction force ( $F_{pl} = 693$  N – standard deviation of 3.3%). This measured value of  $F_{pl}$  is later used to study the rheological behaviour of the studied viscoplastic paste.

### 3.2. Friction force data analysis

The aim of the data analysis is to obtain the relationship between the ram velocity and the friction stress acting along the extruder barrel wall as proposed by eq. (3).

The friction stress value is obtained from the linear part of the evolution of the total force (or the friction force) versus the remaining billet length  $L_B$  as proposed in the previous section and as shown in figure 6 for soft modelling clay. As expected, the slope of the curve does not depend on the extrusion ratio  $d/D$  but is influenced by the ram velocity. From figure 6, it is observed that the computed slope values for different  $d/D$  and same ram velocity are very close.

In figure 7, computed friction stress  $K_w$  is plotted versus the ram velocity for the three tested materials. The best fit of the friction law is given for each of them. We note that the friction law given by eq. (3) is able to describe the friction behaviour of all tested materials as the  $R^2$  coefficient is always higher than 0.99. In order to ensure the accuracy of the proposed method (geometry non-dependency) two extruder barrel diameters were tested. Both diameters



provide the same  $K_w$  values. This confirms the consistency of the proposed method as it does not depend on the extruder geometry, but seems to provide only material friction parameters. It should be noted that the extruder wall roughness is the same in both cases (same steel and same machining to obtain an average roughness of  $3\text{ }\mu\text{m}$ ). Such parameters could have large effects on the measured friction stress, but this is out of scope of the present work (Hoang et al. 2010).

For soft modelling clay, the obtained friction yield stress value is  $31 \pm 2\text{ kPa}$ . This value is close to those obtained with rotating smooth cylinder and back extrusion technique given in section 2.1 (deviation of respectively 3 and 15%). For kaolin, extrusion tests provide a friction yield stress of  $8.7 \pm 1\text{ kPa}$ . This is close the values obtained with the back extrusion technique and smooth cylinder given in section 2.1 (maximum deviation of 9%).

### 3.3. Shaping force analysis

The required pressure drop to ensure the flow of a visco-plastic fluid through an extruder die is commonly modelled by two contributions: The friction forces acting on the material/die interface and the force required for the internal bulk deformation (Benbow and Bridgwater 1993; Benbow et al. 1991).

In our case, the recorded shaping force  $F_{pl}$  required to ensure the flow in the tapered die land (as we considered that the dead zone acts as a conical convergent die) is precisely the sum of three contributions:

- The force required for bulk deformation  $F_{pl,1}$ . It corresponds to the plastic work needed to reduce the billet diameter.
- The force required to overcome the friction on the dead zone which is considered here as a tapered die  $F_{pl,2}$ .
- The force required to overcome the friction on the exit orifice surface  $F_{pl,3}$ .

The analysis of the force required for the plastic work to reduce the diameter of the material billet ( $F_{pl,1}$ ) has been the subject of numerous studies. The most used data analysis is given by Benbow and Bridgwater (Benbow and Bridgwater 1993) and have been used successfully to describe the flow of many materials (Alfani and Guerrini 2005; Basterfield et al. 2005; Li and Bridgwater 2000; Mascia et al. 2006; Rabideau et al. 2010; Zhou and Li 2005a; Zhou and Li 2005b). This equation writes:

$$F_{pl,1} = \frac{\pi D^2}{2} \cdot (\sigma_0 + \alpha V^{n_{BB}}) \ln\left(\frac{D}{d}\right) \quad (6)$$

Where  $\sigma_0$  is considered as the elongational yield stress,  $\alpha$  and  $n_{BB}$  are fitting parameters which depend on the material rheological behaviour. As proposed by Adams et al. (Adams et al. 1997), for a material respecting the Von Mises criterion, the plastic elongational yield stress is equal to  $3^{1/2}\tau_0$ . The main limitation of this model is that  $\alpha$  and  $n_{BB}$  are not material intrinsic parameters.

Basterfield et al. attempt to improve the modelling of the velocity influence on the extrusion force. This model is adapted from the Gibson equation to be able to describe viscoplastic fluids (Basterfield et al. 2005). Assuming a spherically convergent flow (with a dead zone angle of  $45^\circ$ ) and neglecting the contribution due to shear, the author proposed an alternative modelling. They considered the modelling of the flow in a conical duct with an angle around  $45^\circ$  where the shear contribution can be neglected. Finally, the author derived the equation (the transitions between conical and cylindrical flows at both the dead zone and the exit orifice entrance are neglected):

$$F_{pl,1} = \frac{\pi D^2}{4} \cdot \left[ 2\sqrt{3}\tau_0 \ln\left(\frac{D}{d}\right) + \frac{2k_s \sqrt{3}^{n_s+1}}{3n_s \cdot 2^{n_s}} \left(\frac{2V \cdot D^2}{d^3}\right)^{n_s} \sin \theta (1 + \cos \theta)^{n_s} (1 - (d/D)^{3n_s}) \right] \quad (7)$$

With  $n_s$  and  $k_s$  represent respectively the flow index and the flow consistency. We note that when the ram velocity tends to 0, eq. (7) reduces to eq. (6). Equation (7) is finally used in the present study to evaluate the force contribution linked with internal deformation.

Then, the force required to overcome the friction on the tapered dead zone surface is computed using the modelling given by Benbow and co-authors (Benbow and Bridgwater 1993; Benbow et al. 1991). It is important to note that the friction stress acting on the dead zone surface differ from the friction stress acting on the steel barrel (the interface roughness is different). Moreover, in this particular case, the tribological behaviour implies a material/material interface. As a consequence, it seems rational to consider the friction at such interface as a thin localized shear band. Thus, as used for squeeze geometry (Sherwood and Durban 1996, 1998; Engmann et al. 2005), it is assumed that the friction stress at the extruder barrel is a fraction of the friction stress at the dead zone interface. We define a coefficient  $m$  as the ratio of the friction stress at the extruder barrel to the friction stress at the dead zone interface. Moreover this coefficient  $m$  tends to  $K_{w0}/\tau_0$  when the interfacial velocity tends to 0. The coefficient  $m$  can be expressed as follow:

$$m = \frac{K_w(\text{steel surface})}{K_w(\text{dead zonesurface})} = \frac{K_{w0}}{\tau_0} \quad (8)$$

This coefficient allows us to write the friction force acting on the tapered dead zone surface. The final expression is given by the Benbow and co-authors modelling combined with eqs. (3) and (8) (Benbow and Bridgwater 1993; Benbow et al. 1991):

$$F_{Pl,2} = \frac{1}{m} \frac{\pi D^2}{4} \left[ K_{w0} \cot \theta \ln \frac{d}{D} + k_{fr} V^{n_{fr}} \frac{D^{2n_{fr}}}{d^{2n_{fr}}} \left( 1 - \left( \frac{d}{D} \right)^{2n_{fr}} \right) \right] \quad (9)$$

It can be noted that this assumes that the slip layer behaviour is the same against the extruder barrel and against the static zone. However, it can be considered that the power law index taken for the material/material interface can be equal to  $n_s$  as it concerns a material/material interface. At least, the power law index ranges between  $n_{fr}$  and  $n_s$ . This could have some noticeable impact that would be discussed at the end of the section.

The third contribution which corresponds to the friction along the die orifice steel surface ( $R_t = 3\mu\text{m}$ ) is commonly written using a simple force balance equation:

$$F_{Pl,3} = \pi d L_O \left[ K_{w0} + k_{fr} V^{n_{fr}} \frac{D^{2n_{fr}}}{d^{2n_{fr}}} \right] \quad (10)$$

Finally, the shaping force  $F_{pl}$  is provided by the summation of the three contributions:

$$F_{pl} = F_{Pl,1} + F_{Pl,2} + F_{Pl,3} \quad (11)$$

For the three tested materials, it is then possible to highlight the rheological parameters (i.e.  $\tau_0$ ,  $k_s$  and  $n_s$ ) which provide the best fit between experiments and modelling. Results are shown on figures 8 to 10. Those curves show that the proposed modelling is able to provide an estimation of the rheological parameters without extruder geometry dependency. This conclusion is clearly presented on figure 11 where the modelled values of the shaping force  $F_{pl}$  are plotted versus the measured ones. The correlation between modelling and experiments is very good ( $R^2=0.99$ ). The Basterfield et al. analysis applied to the used die geometry and local roughness is suitable for the shaping force analysis. Rheological parameters are listed in the table 1. Shear thinning behaviour characterises the three tested materials. The comparison of the shear yield stress obtained by vane geometry (section 2.1) and Extrusion tests shows that extrusion provides close higher values for the three tested materials. The variation is more significant for of kaolin paste (35%) and cement paste (21%) and is lower for soft modelling clay (11%).

In order to study the effect of the power law index used to compute the friction against the dead zone, the computation is also made using  $n_s$  instead of  $n_{fr}$  in eq. (9). In this case, the obtained consistencies and flow index changes. The consistency  $k_s$  becomes 17.5 kPa.s instead of 11.5 kPa.s for the cement paste, 19.0 kPa instead of 12.8 kPa for the kaolin and 5.1 instead of 16.8 kPa for the soft modelling clay. The flow index  $n_s$  remains at 0.1 for the cement paste but becomes 0.2 instead of 0.11 for the kaolin and 0.9 instead of 0.46 for the soft

modelling clay. Those values provide also a good correlation  $R^2=0.96$ . This shows that the assumption of the friction law against the static zone is important as it largely influences the determination of the consistency and flow index. It can be advised to use conical steel die with the same roughness as the barrel one to validate the use of  $n_{fr}$  in eq. (9).

## 4 Conclusions

In this study, we design a new extruder to study both the rheological and tribological properties of high yield stress materials. According to literature data, the extrusion force can be split into two contributions: the friction force acting along the extruder barrel and the shaping force in the die land. The new device is developed that makes it possible to measure both contributions. The measured friction force  $F_{fr}$  is used to study the material tribology. A simple force balance equation allows us computing the friction stress acting on the barrel wall. For the shaping force  $F_{pl}$ , the Basterfield et al. equation is adapted to our die geometry (conical dead zone which acts as a rough tapered die). The use of our experimental data bank allows us to valid our protocol of data analysis for firm materials. The method is finally used to compute the Herschel-Buckley modelling parameters of the three tested materials (soft modelling clay, kaolin clay and cement-based paste). Shear yield stress results are in agreement with those computed from vane test shear yield stress.

## References

- Adams MJ, Briscoe BJ, Corfield GM, Lawrence CJ, Papathanasiou TD (1997) A finite element analysis of the squeeze flow of an elasto-plastic paste material. *Journal of Non-Newtonian Fluid Mechanics* 71 (1):41-57
- Alfani R, Guerrini GL (2005) Rheological test methods for characterization of extrudable cement-based materials. *Materials and Structures* 38 (2):239-247
- Avitzur B (1983) *Handbook of metal forming processes*. New York

Barnes EC, Wilson DI, Johns ML (2006) Velocity profiling inside a ram extruder using magnetic resonance (MR) techniques. *Chemical Engineering Science* 61 (5):1357-1367  
 Basterfield RA, Lawrence CJ, Adams MJ (2005) On the interpretation of orifice extrusion data for viscoplastic materials. *Chemical Engineering Science* 60 (10):2599-2607  
 Benbow JJ, Bridgwater J (1993) *Paste Flow and Extrusion*. Oxford  
 Benbow JJ, Jazayeri SH, Bridgwater J (1991) The flow of pastes through dies of complicated geometry. *Powder Technology* 65 (1-3):393-401  
 Cheyne A, Barnes J, Wilson DI (2005) Extrusion behaviour of cohesive potato starch pastes: I. Rheological characterisation. *Journal of Food Engineering* 66 (1):1-12  
 Dealy JM (1995) On the significance of pressure relaxations in capillary or slit flow. *Rheologica Acta* 34 (1):115-116  
 Doll G, Händle F, Spiessberger F, Händle F (2007) *Piston Extruders Extrusion in Ceramics*. In: *Engineering Materials and Processes*. Springer Berlin Heidelberg, pp 259-273  
 Engmann J, Servais C, Burbidge AS (2005) Squeeze flow theory and applications to rheometry: A review. *Journal of Non-Newtonian Fluid Mechanics* 132 (1-3):1-27  
 Estellé P, Lanos C, Perrot A (2008) Processing the Couette viscometry data using a Bingham approximation in shear rate calculation. *Journal of Non-Newtonian Fluid Mechanics* 154 (1):31-38  
 Estellé P, Lanos C, Perrot A, Servais C (2006) Slipping zone location in squeeze flow. *Rheologica Acta* 45 (4):444-448  
 Gibson AG (1988) Converging dies In: Collyer, A.A., Clegg, D.W. (Eds.), *Rheological Measurements*. Barking  
 Götz J, Zick K, Kreibich W (2003) Possible optimisation of pastes and the according apparatus in process engineering by MRI flow experiments. *Chemical Engineering and Processing* 42 (7):517-534  
 Hill R (1950) *Mathematical theory of plasticity*. Oxford  
 Hoang VH, Melinge Y, Perrot A, Rangeard D Local properties of clay based materials under tribological testing. In: 6th World Congress on Particles Technology Nuremberg, Germany, 2010. p 00577  
 Horrobin DJ (1999) *Theoretical aspects of Paste Extrusion*. University of Cambridge, Cambridge  
 Horrobin DJ, Nedderman RM (1998) Die entry pressure drops in paste extrusion. *Chemical Engineering Science* 53 (18):3215-3225  
 Jay P, Magnin A, Piau JM (2002) Numerical Simulation of Viscoplastic Fluid Flows Through an Axisymmetric Contraction. *Journal of Fluids Engineering* 124:700-705  
 Kobayashi S, Thomsen EG (1963) Upper- and lower-bound solutions to axisymmetric compression and extrusion problems. *International Journal of Mechanical Sciences*, 7:127-143  
 Li YY, Bridgwater J (2000) Prediction of extrusion pressure using an artificial neural network. *Powder Technology* 108 (1):65-73  
 Liddel PV, Boger DV (1996) Yield stress measurements with the vane. *Journal of Non-Newtonian Fluid Mechanics* 63 (2-3):235-261  
 Mankar RB, Graczyk J, Gonzalez-Alvarez A, Buggisch H Capillary rheometry studies on wall slip flow of pastes. In: XIVth International Congress on Rheology, Seoul, Korea, August 22-27, 2004 2004. pp RE 43-41  
 Martin PJ, Wilson DI, Bonnett PE (2006) Paste extrusion through non-axisymmetric geometries: Insights gained by application of a liquid phase drainage criterion. *Powder Technology* 168 (2):64-73

545 Mascia S, Patel MJ, Rough SL, Martin PJ, Wilson DI (2006) Liquid phase migration in the  
 546 extrusion and squeezing of microcrystalline cellulose pastes. *European Journal of*  
 547 *Pharmaceutical Sciences* 29 (1):22-34  
 548 Mimoun M, Aouadja FZ (2004) Rheometrical exploitation of experimental results obtained  
 549 from new simulation device of extrusion on clay paste. *Materials and Structures* 37  
 550 (3):193-201  
 551 Mitsoulis E, Delgadillo-Velazquez O, Hatzikiriakos SG (2007) Transient capillary rheometry:  
 552 Compressibility effects. *Journal of Non-Newtonian Fluid Mechanics* 145 (2):102-108  
 553 Mitsoulis E, Hatzikiriakos SG (2009) Steady flow simulations of compressible PTFE paste  
 554 extrusion under severe wall slip. *Journal of Non-Newtonian Fluid Mechanics* 157  
 555 (1):26-33  
 556 Park H, Lim S, Laun H, Dealy J (2008) Measurement of pressure coefficient of melt  
 557 viscosity: drag flow versus capillary flow. *Rheologica Acta* 47 (9):1023-1038  
 558 Perrot A, Lanos C, Estellé P, Melinge Y (2006) Ram extrusion force for a frictional plastic  
 559 material: model prediction and application to cement paste. *Rheologica Acta* 45  
 560 (4):457-467  
 561 Perrot A, Lanos C, Melinge Y, Estellé P (2007) Mortar physical properties evolution in  
 562 extrusion flow. *Rheologica Acta* 46 (8):1065-1073  
 563 Perrot A, Melinge Y, Rangeard D, Estellé P, Lanos C (2011) The back extrusion test as a  
 564 technique for determining the rheological and tribological behaviour of yield stress  
 565 fluids. *Applied Rheology* 21 (5):53642  
 566 Perrot A, Rangeard D, Melinge Y, Estellé P, Lanos C (2009) Extrusion criterion for firm  
 567 cement-based materials. *Applied Rheology* 19 (5):53042  
 568 Rabideau BD, Moucheron P, Bertrand F, Rodts S, Roussel N, Lanos C, Coussot P (2010)  
 569 The extrusion of a model yield stress fluid imaged by MRI velocimetry. *Journal of*  
 570 *Non-Newtonian Fluid Mechanics* 165 (7-8):394-408  
 571 Rahman L, Rowe P, Cheyne A, Wilson DI (2002) Ram Extrusion of Potato Starch Dough  
 572 Through Multi-Holed Dies. *Food and Bioproducts Processing* 80 (1):12-19  
 573 Roussel N, Lanos C (2003) Plastic Fluid Flow Parameters Identification Using a Simple  
 574 Squeezing Test  
 575 *Applied Rheology* 13:132  
 576 Sherwood JD, Durban D (1996) Squeeze flow of a power-law viscoplastic solid. *Journal of*  
 577 *Non-Newtonian Fluid Mechanics* 62 (1):35-54  
 578 Sherwood JD, Durban D (1998) Squeeze-flow of a Herschel-Bulkley fluid. *Journal of Non-*  
 579 *Newtonian Fluid Mechanics* 77 (1):115-121  
 580 Srinivasan R, DeFord D, Shah SP (1999) The use of extrusion rheometry in the development  
 581 of extruded fiber-reinforced cement composites. *Concrete Science and engineering* 1  
 582 (1):26-36  
 583 Toplak T, Tabuteau H, de Bruyn JR, Coussot P (2007) Gravity draining of a yield-stress fluid  
 584 through an orifice. *Chemical Engineering Science* 62 (23):6908-6913  
 585 Toutou Z, Roussel N, Lanos C (2005) The squeeze test: A tool to identify firm cement-based  
 586 material's rheological behaviour and evaluate their extrusion ability. *Cement and*  
 587 *Concrete Research* 35 (10):1891-1899  
 588 Wildman RD, Blackburn S, Benton DM, McNeil PA, Parker DJ (1999) Investigation of paste  
 589 flow using positron emission particle tracking. *Powder Technology* 103 (3):220-229  
 590 Yu AB, Bridgwater J, Burbidge AS, Saracevic Z (1999) Liquid maldistribution in particulate  
 591 paste extrusion. *Powder Technology* 103 (2):103-109  
 592 Zhou X, Li Z (2005a) Characterization of rheology of fresh fiber reinforced cementitious  
 593 composites through ram extrusion. *Materials and Structures* 38 (1):17-24

Zhou XM, Li ZJ (2005b) Characterization rheology of fresh short fiber reinforced cementitious composite through capillary extrusion. *Journal of Materials in Civil Engineering* 17 (1):28-35

Zienkiewicz OC, Jain PC, Onate E (1977) Flow of solids during forming and extrusion: Some aspects of numerical solutions. *International Journal of Solids and Structures* 14:15-38

## Table Caption

Table 1: Rheological and tribological modelling parameters obtained with vane tests and extrusion for the three tested materials.

## Figure Captions

Figure 1: Force distribution in the extrusion flow of high yield stress fluid

Figure 2: Dead zone length observation with soft modelling clay test extrusion (Ram velocity  $1 \text{ mm.s}^{-1}$ ,  $d=16 \text{ mm}$  and  $D=43.3 \text{ mm}$ ). Comparison with modelled conical dead zones.

Figure 3: Friction force measurement system in the designed die.

Figure 4: Typical evolution of the total extrusion force versus the remaining billet length. Test performed on soft modelling clay,  $D=55.3 \text{ mm}$ ;  $d/D=0.36$ ;  $V = 1 \text{ mm.s}^{-1}$ .

Figure 5: Evolution of the friction and total extrusion force versus the remaining billet length measured with the developed extruder. Test performed on Soft modelling clay:  $D=43.3 \text{ mm}$ ,  $d/D=0.36$ ,  $V=1 \text{ mm.s}^{-1}$ .

Figure 6: Total extrusion force versus remaining billet length of soft modelling clay. Tests performed for  $D = 43.3 \text{ mm}$ . Slopes of linear fitting  $\Delta F/\Delta L_B$  are: 4.12 ( $R^2=0.99$ ) for  $d = 8 \text{ mm}$  and  $V = 0.1 \text{ mm.s}^{-1}$ ; 5.21 ( $R^2=0.96$ ) for  $d = 8 \text{ mm}$  and  $V = 1 \text{ mm.s}^{-1}$ ; 3.85 ( $R^2=0.99$ ) for  $d = 20 \text{ mm}$  and  $V = 0.1 \text{ mm.s}^{-1}$ ; 5.06 ( $R^2=0.97$ ) for  $d = 20 \text{ mm}$  and  $V = 1 \text{ mm.s}^{-1}$  ;

Figure 7: Friction law obtained for the three tested materials.



Figure 8: Modelled and experimental values of shaping force  $F_{pl}$  for soft modelling clay versus the ram advance.  $\tau_0 = 56.8$  kPa ;  $k_s = 16.7$  kPa.s<sup>ns</sup> ;  $n_s = 0.46$  are the values providing the best fit for the modelling. Tests performed with  $D = 44.3$  mm and  $D=55.3$  mm.

Figure 9: Modelled and experimental values of shaping force  $F_{pl}$  for kaolin paste versus the ram advance.  $\tau_0 = 39.1$  kPa ;  $k_s = 12.8$  kPa.s<sup>ns</sup> ;  $n_s = 0.11$  are the values providing the best fit for the modelling. Tests performed with  $D = 44.3$  mm and  $D=55.3$  mm.

Figure 10: Modelled and experimental values of shaping force  $F_{pl}$  for cement paste versus the ram advance.  $\tau_0 = 19.0$  kPa ;  $k_s = 11.5$  kPa.s<sup>ns</sup> ;  $n_s = 0.1$  are the values providing the best fit for the modelling. Tests performed with  $D = 44.3$  mm and  $D=55.3$  mm.

Figure 11: Correlation between the modelled shaping force value  $F_{pl}$  and the experimental value for the three tested materials.

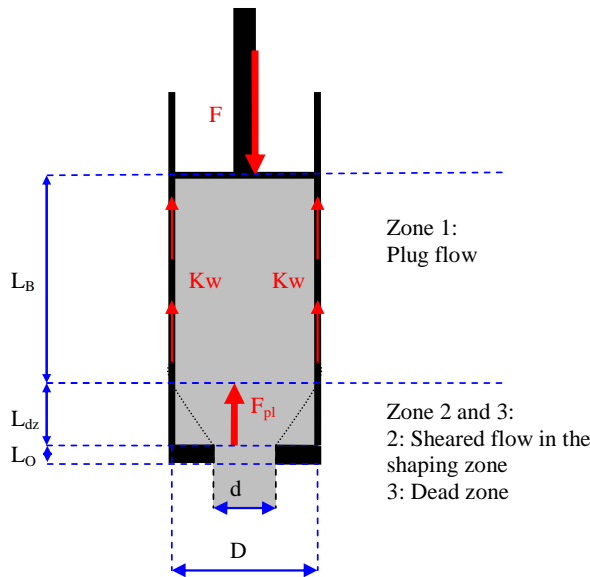


Figure 1

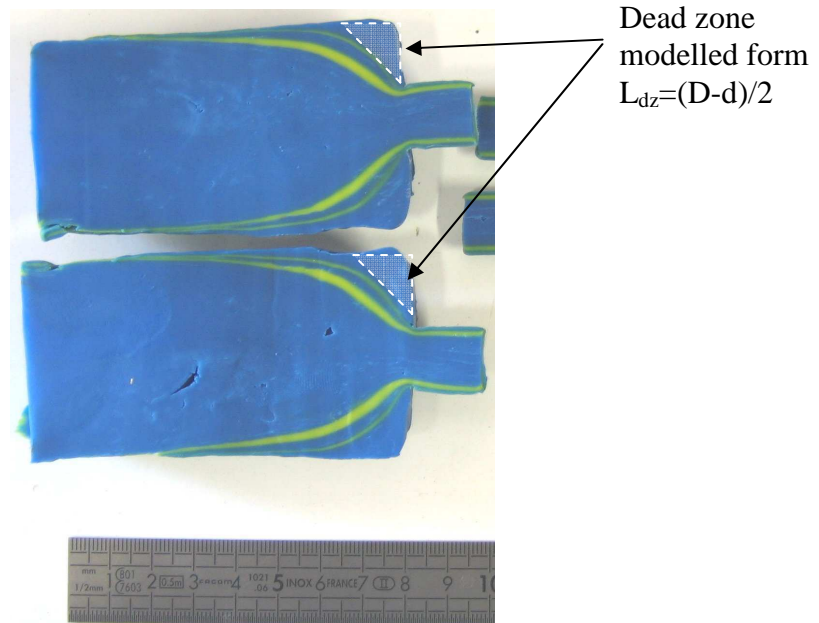


FIGURE 2

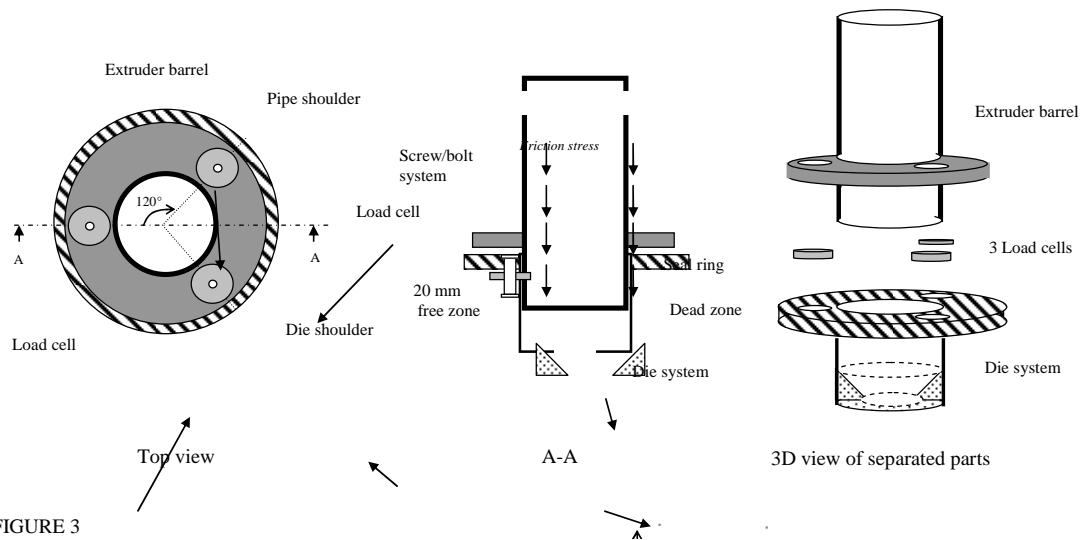
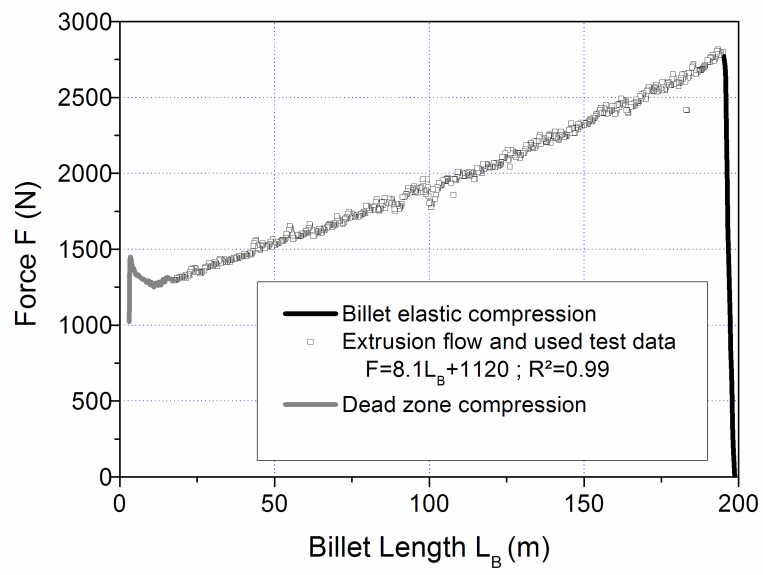


FIGURE 3

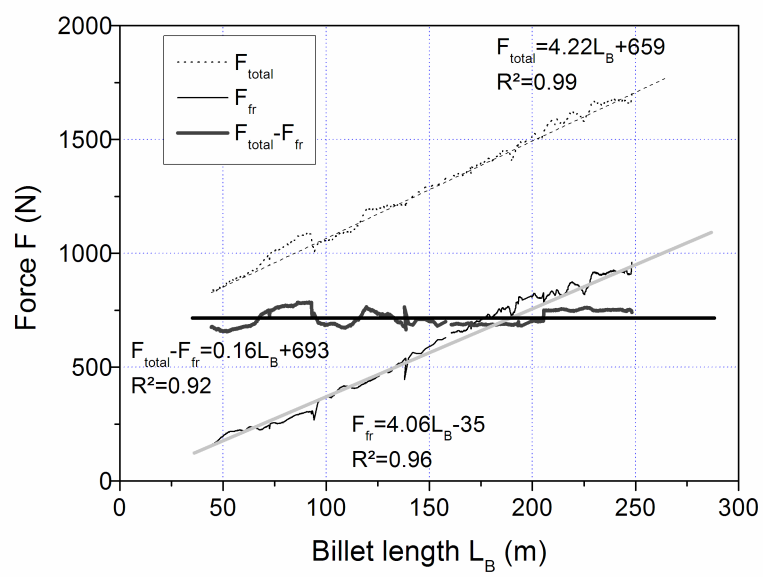
Figure 4



646

647

Figure 5



648

Figure 6

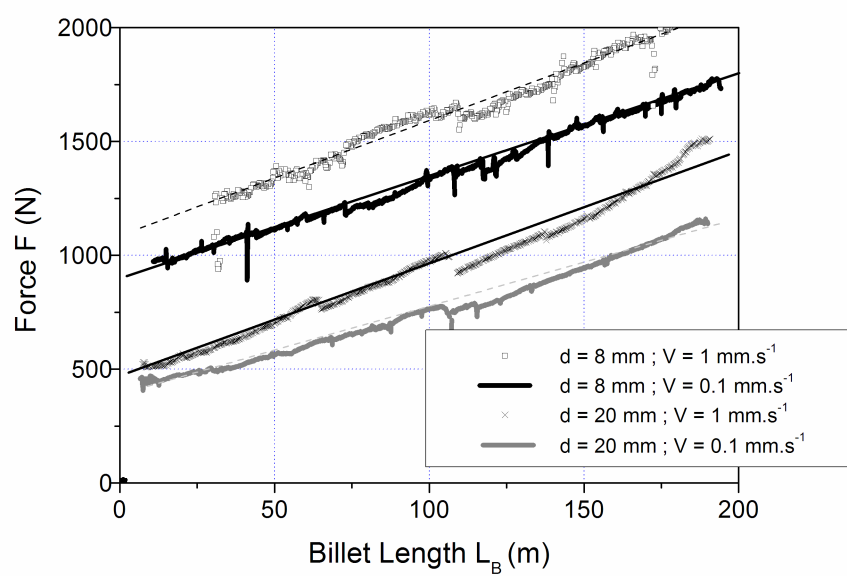


Figure 7

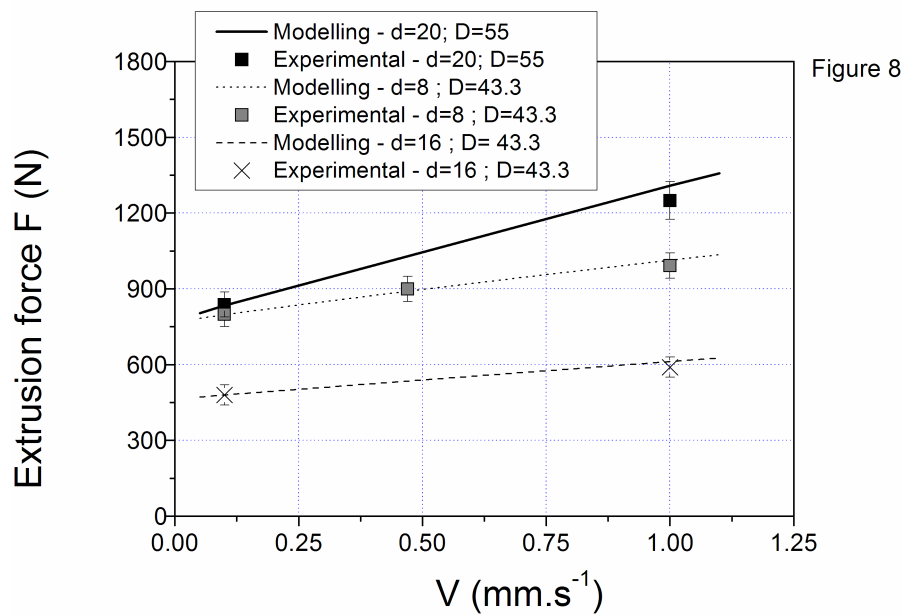
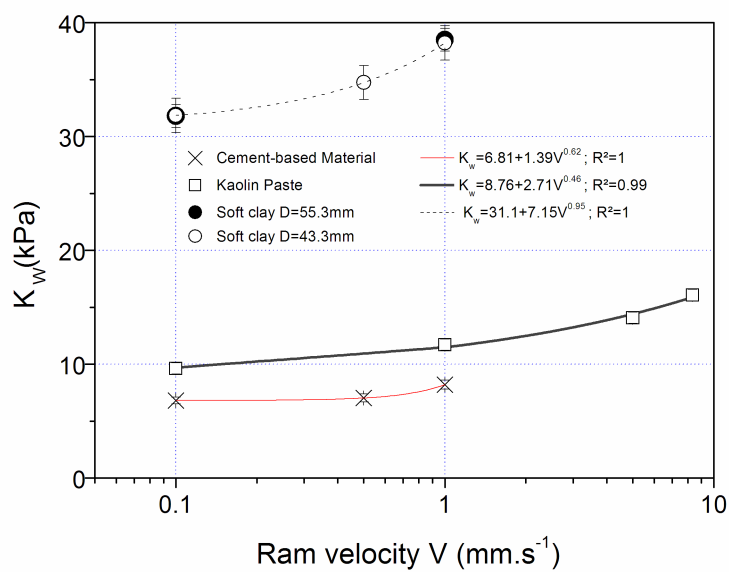
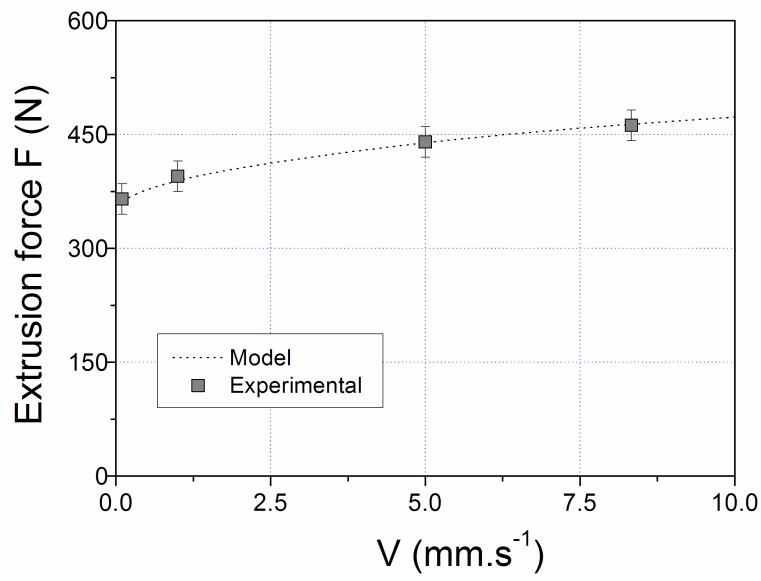
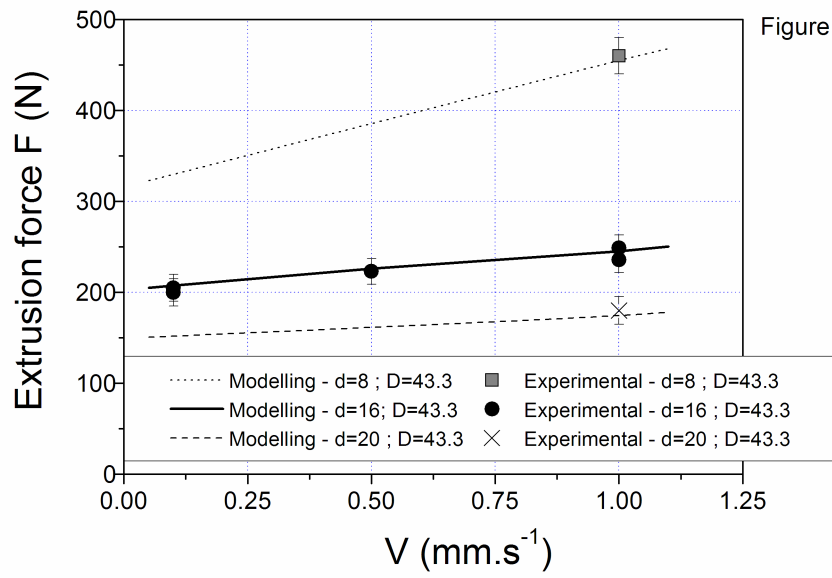


Figure 9



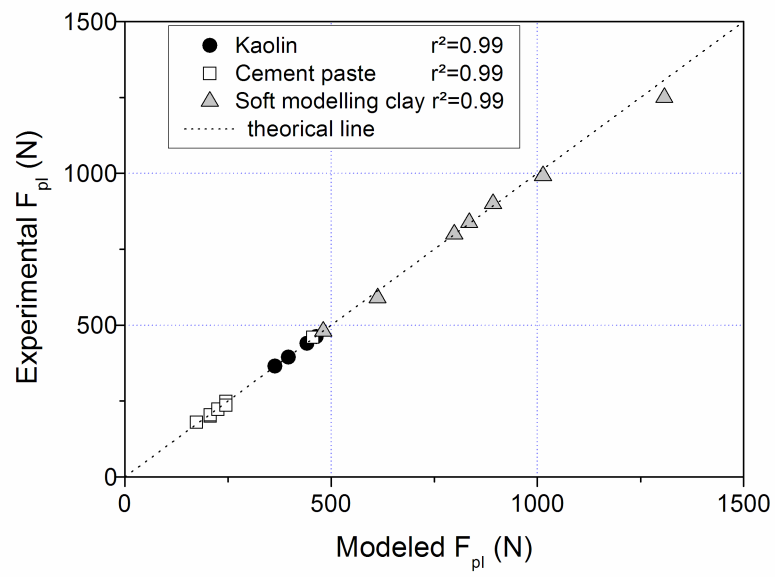
652

Figure 10



653

Figure 11



654